Dyes and Pigments 86 (2010) 206–216

Contents lists available at ScienceDirect

Dyes and Pigments

journal homepage: www.elsevier.com/locate/dyepig

The synthesis of 1,8-naphthalimide groups containing imidazolium salts/ionic liquids using I^-, PF_6^-, $TFSI^-$ anions and their photophysical, electrochemical and thermal properties

Saliha Ozdemir [a], Canan Varlikli [a,*], Ilker Oner [a], Kasim Ocakoglu [a,b], Siddik Icli [a]

[a] Ege University, Solar Energy Institute, 35100 Bornova-Izmir, Turkey
[b] Mersin University, Tarsus Technical Education Faculty, 33480 Tarsus-Mersin, Turkey

ARTICLE INFO

Article history:
Received 23 September 2009
Received in revised form
8 January 2010
Accepted 12 January 2010
Available online 4 February 2010

Keywords:
Ionic salt
Imidazolium
Naphthalimide
Photostability
Quenching
Ionic liquid

ABSTRACT

1,8-Naphthalimide groups containing imidazolium iodide salts of different alkyl chain length on the imidazole group were synthesized. Hexafluorophosphate and bis(trifluoromethanesulfonyl)imide salts were obtained by ion exchange reactions. The synthesized salts were characterized using a variety of spectroscopic techniques. Fluorescence emission quenching of iodide and bis(trifluoromethanesulfonyl) imide salts were studied using a ruthenium dye, whilst that of hexafluorophosphate salts were performed using tris(8-hydroxyquinoline)aluminum. Calculated fluorescence quenching rate constants were as high as $10^{14}\,M^{-1}\,s^{-1}$ and values of the Gibbs free energy of electron transfer were [−32.04/−33.68], [−17.52/−20.74] and [−26.50/−30.89] kcal mol^{-1} for the iodide, hexafluorophosphate and bis(trifluoromethanesulfonyl) imide salts, respectively. The thermal stability of the synthesized salts was high especially in the case of bis (trifluoromethanesulfonyl)imide salts for which values of 470–498 °C were achieved. Photostability studies of hexafluorophosphate and bis(trifluoromethanesulfonyl)imide salts were also performed; calculated photodegradation half-life values ranged from 19.25 to 48.12 h.

1. Introduction

In recent years, ionic liquids (ILs) have received much attention because of their unique characteristics such as low volatility, non-flammability, high thermal stability, high ionic conductivity and broad operating temperature range [1–6]. Typically, ionic liquids are liquid at low temperature (<100 °C) and consist of a bulky, asymmetric organic cation (e.g. imidazolium or pyridinium ions, also alkylphosphonium and alkylammonium ions) and a smaller inorganic anion. The compounds possess high electrochemical stability and high ionic conductivity [7–12]. Appropriate choices of the anion/cation combination permit the tuning of properties of ionic liquids such as miscibility with water and other solvents, dissolution ability, polarity, viscosity and density.

Ionic liquids based on imidazolium salts have been studied extensively as non-volatile electrolytes in nc-TiO_2 based dye sensitized solar cells (DSSCs), owing to their good stability and high ionic conductivity [13–17]. Recently, imidazolium ionic liquids and organic salts have been used in organic light-emitting devices (OLEDs) as a means of enhancing the efficiency of such devices as a result of improved charge injection [18,19]. It has been reported that using imidazolium ionic liquid in thin film transistors as an electrolyte component improves device characteristics [20]; investigations into the use of imidazolium based ILs for capacitors, fuel cells and batteries have been carried out [4,21–25].

Naphthalimide derivatives, which are of interest in various scientific and technological fields, were chosen because of their excellent photophysical and photochemical properties. The compounds enjoy use as dyes for organic solar cells [26], fluorescent dyes for solar energy collectors [27], organic light-emitting diodes and organic field effect transistors as n-type semiconductors [28,29], fluorescent markers for medical and biological purposes [30] (such as potential HIV drugs, cell makers, DNA-cleaving agents), laser dyes [31] and liquid-crystal additives for electro optical displays of the guest-host type [32,33].

This paper concern the synthesis of a series of novel imidazolium salts with the naphthalimide functional group attached to the imidazolium cation, employing iodide (I^-), hexafluorophosphate (PF_6^-) and bis(trifluoromethanesulfonyl)imide ($TFSI^-$) as anions. The salts were characterized using spectroscopic, electrochemical and thermal methods; some of the salts can be considered as ionic liquids since they have melting points <100 °C. The major focus of this work was to investigate novel imidazolium salts/ionic liquids

* Corresponding author. Tel.: +90 232 3886025; fax: +90 232 3886027.
E-mail address: canan.varlikli@ege.edu.tr (C. Varlikli).

0143-7208/$ – see front matter © 2010 Elsevier Ltd. All rights reserved.
doi:10.1016/j.dyepig.2010.01.005

comprising an electron-deficient 1,8-naphthalimide group attached to the imidazole ring. Naphthalimide groups can be use in OLEDs as electron transfer and hole blocking material [34,35]. Together with the ionic imidazolium group, they may form a donor-acceptor couples and enhance charge injection in an OLED's. The I^- and $TFSI^-$ salts of the compounds may be used as electrolyte components or solid electrolytes in DSSCs. In addition to these and above mentioned application areas, the synthesized salts may find application in other fields where naphthalimides and imidazolium salts are used; such as, biological applications [36,37].

2. Experimental

2.1. Instruments

UV–Vis and fluorescence spectra were recorded in a 1 cm path length quartz cell by using Analytik Jena S 600 UV–Vis and PTI-QM1 luminescence spectrophotometers, respectively. The infrared (IR) spectra were obtained by using Perkin–Elmer, Spectrum BX-FTIR spectrophotometer, ^{1}H NMR, ^{13}C NMR, ^{19}F-NMR and ^{31}P-NMR spectra were measured on a Bruker 400 MHz spectrometer. Electrochemical studies were carried out with a CH Instrument 660 B Model Electrochemical Workstation. Thermal properties were analyzed by the use of Perkin Elmer Pyris 6 DSC and Pyris 6 TGA. Electrospray mass spectra were obtained using an LCT Premier Mass Spectrometer from Micromass Technologies. Conductivity measurements were performed by using Keithley Source-meter Model 2400 at room temperature. Aluminum depositions were performed in a thermal evaporator plant attached in MBRAUN 200B glove box system. Laurell WS-400B-6NPP-LITE spin processor was used in the preparation of the films.

2.2. Materials

The commercial reagents; 1,8-naphthalic anhydride, 1-(3-aminopropyl)imidazole, alkyl iodide compounds (ethyl, n-butyl, n-hexyl, n-octyl, n-decyl iodide), lithium bis(trifluoromethanesulfonyl)imide salt (LiTFSI; caution: avoid oxidants and acids), ammonium haxafluorophosphate salt (NH_4PF_6) and 1-methyl-3-propylimidazolium iodide (PMII) were supplied from Aldrich and used without any treatment. The organic solvents used for synthesis and spectroscopic measurements [chloroform ($CHCl_3$), ethanol (EtOH), acetonitrile (MeCN), toluene, N,N-dimethylformamide (DMF)] were all of spectrophotometric grade. The other solvents used for purification and crystallization processes [dichloromethane (CH_2Cl_2), hexane, acetone, acetonitrile (MeCN)] were used after distillation. Aluminum (Al) used in conductivity measurements was supplied from Aldrich.

2.3. Synthesis of the starting material, N-(3-propylimidazole)-1,8-naphthalene monoimide, [SO]

1-(3-Aminopropyl)imidazole (6 mL, 50 mmol) and DMF (20 mL) were added to a two-necked round-bottomed flask fitted with a reflux condenser and the solution was stirred. To this stirring solution, 1,8-naphthalic anhydride (1.1 g, 5.5 mmol) was added slowly in small pieces to prevent the aggregation. The mixture was heated to reflux for 24 h. Then, the solvent was decanted and a light brown product was obtained. The crude product was washed with acetone (3 × 20 mL) to remove the unreacted starting materials and crystallized from CH_2Cl_2/Hexane (15/20 mL) mixture. The reaction progress was screened by TLC control over silica gel plate ($CHCl_3$/CH_3OH, 3:1). ^{1}H NMR (δ_H, *ppm, 400 MHz, CDCl$_3$*): 8.60–8.58 (d, 2H, J = 7.2 Hz, Ar); 8.22–8.20 (d, 2H, J = 8.4 Hz, Ar); 7.77–7.73 (t, 2H, J = 7.8 Hz, Ar); 7.54 (s, 1H, Ar); 7.03–7.00 (d, 2H, J = 10.8 Hz, Ar); 4.25–4.22 (t, 2H, J = 7.0 Hz); 4.09–4.06 (t, 2H, J = 7.4 Hz); 2.30–2.22 (m, 2H, J = 7.2). ^{13}C NMR (δ_C, *ppm, 400 MHz, CDCl$_3$*): 164.4, 137.4, 134.4, 131.8, 131.6, 129.8, 128.3, 127.2, 122.6, 118.9, 45.2, 37.9, 29.9. IR (500–4000 cm^{-1}, KBr pellet): 3082 (ν_{C-H}, aromatic), 1689 ($\nu_{C=N}$), 1649 ($\nu_{C=O}$, aromatic). Yield: 62.78%.

2.4. Synthesis and characterization of the imidazolium iodide salts

Imidazolium iodide salts were synthesized through the *N*-alkylation reaction [38] (Fig. 1) between SO molecule and corresponding alkyl iodide compound (RI, R = ethyl, n-butyl, n-hexyl, n-octyl, n-decyl). Synthesized iodide salts and their codes used throughout the text are given in Table 1.

Under dry nitrogen atmosphere, SO starting material (0.61 g, 2 mmol) and toluene (20 mL) were added to a round-bottomed flask fitted with a reflux condenser and alkyl iodide compound (3 mmol) was added to the stirring solution. The mixture was heated to 90 °C, and left to stir for approximately 2 days. After 2 days, the solvent was decanted and yellowish powder products were obtained. SO8-I and SO10-I compounds were obtained as a brown gel before purification. All products were washed with diethylether (3 × 10 mL) and crystallized from CH_2Cl_2/Diethylether (15/20 mL) mixture.

SO2-I: ^{1}H NMR (δ_H, *ppm, 400 MHz, DMSO*): 9.18 (s, 1H, Ar); 8.45 (d, 2H, J = 1.6 Hz, Ar); 8.43 (d, 2H, J = 2.8 Hz, Ar); 7.87–7.83 (t, 2H, J = 7.8 Hz, Ar); 7.80 (s, 1H, Ar); 7.79 (s, 1H, Ar); 4.28–4.24 (t, 2H, J = 7.6 Hz); 4.20–4.15 (q, 2H, J = 7.5 Hz); 4.09–4.06 (t, 2H, J = 6.4 Hz); 2.27–2.21 (m, 2H, J = 7.1 Hz); 1.41–1.38 (t, 3H, J = 7.2 Hz). ^{13}C NMR (δ_C, *ppm, 100 MHz, DMSO*): 164.3, 136.6, 135.1, 131.9, 131.4, 128.1, 127.9, 123.1, 122.8, 122.7, 47.7, 44.9, 37.4, 29.0, 15.7. IR (500–4000 cm^{-1}, KBr pellet): 3060 (ν_{C-H}, aromatic); 2982 (ν_{C-H}, aliphatic); 1702 ($\nu_{C=O}$); 1659 ($\nu_{C=N}$); 783(ν_{C-H}, aromatic). TOF MS ES$^+$: *m/z* calc. for $[C_{20}H_{20}N_3O_2]^+$: 334.1556; found: 334.1526. TOF MS ES$^-$: *m/z* calc. for $[I]^-$: 126.9045; found: 126.9042. Yield: 80%.

SO4-I: ^{1}H NMR (δ_H, *ppm,* 400 *MHz*, *CDCl$_3$*): 10.03 (s, 1H, Ar); 8.43–8.41 (d, 2H, J = 7.2 Hz, Ar); 8.15–8.13 (d, 2H, J = 8.4 Hz, Ar); 7.84 (s, 1H, Ar); 7.69 (s, 1H, Ar); 7.69–7.65 (t, 2H, J = 7.8 Hz, Ar); 4.53–4.50 (t, 2H, J = 6.6 Hz); 4.43–4.40 (t, 2H, J = 7.4 Hz); 4.18–4.15 (t, 2H, J = 6.4 Hz); 2.47–2.40 (m, 2H, J = 6.5 Hz); 2.00–1.93 (m, 2H, J = 7.5 Hz); 1.46–1.40 (m, 2H, J = 7.6 Hz); 0.99–0.95 (t, 3H, J = 7.4 Hz). ^{13}C NMR (δ_C,*ppm*, 400 *MHz*, *CDCl$_3$*): 164.4; 136.7, 134.5, 131.6, 131.5, 128.1, 127.2, 122.9, 122.8, 122.1, 50.3, 48.2, 37.0, 32.3, 29.3, 19.7, 13.7. IR (500–4000 cm^{-1}, KBr pellet): 3089 (ν_{C-H}, aromatic); 2966–2934 (ν_{C-H}, aliphatic); 1696 ($\nu_{C=O}$); 1656; ($\nu_{C=N}$); 784 (ν_{C-H}, aromatic). TOF MS ES$^+$: *m/z* calc. for $[C_{22}H_{24}N_3O_2]^+$: 362.1869; found: 362.1953. TOF MS ES$^-$: *m/z* calc. for $[I]^-$: 126.9045; found: 126.9029. Yield: 69%.

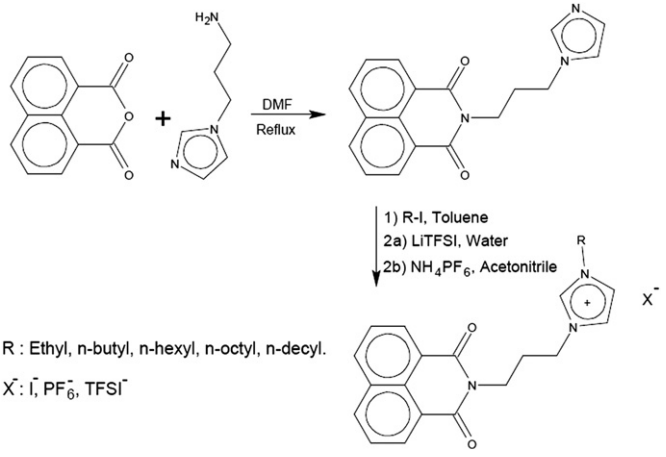

Fig. 1. Synthetic route of the starting material and synthesized salts.

Table 1
Synthesized salts and their codes according to alkyl chain length on the imidazole group.

R (alkyl group)	Code (I^- salts)	Code ($TFSI^-$ salts)	Code (PF_6^- salts)
ethyl ($-C_2H_5$)	SO2-I	SO2-TFSI	SO2-PF_6
n-butyl ($-C_4H_9$)	SO4-I	SO4-TFSI	SO4-PF_6
n-hexyl ($-C_6H_{13}$)	SO6-I	SO6-TFSI	SO6-PF_6
n-octyl ($-C_8H_{17}$)	SO8-I	SO8-TFSI	SO8-PF_6
n-decyl ($-C_{10}H_{21}$)	SO10-I	SO10-TFSI	SO10-PF_6

SO6-I: ^{1}H NMR (Fig. 2) (δ_H, *ppm*, 400 *MHz*, *$CDCl_3$):* 9.95 (s, 1H, Ar); 8.36–8.34 (d, 2H, $J = 6.8$ Hz, Ar); 8.08–8.06 (d, 2H, $J = 8$ Hz, Ar); 7.79 (s, 1H, Ar); 7.61 (s, 1H, Ar); 7.61–7.57 (t, 2H, $J = 7.8$ Hz, Ar); 4.46–4.43 (t, 2H, $J = 6.6$ Hz); 4.35–4.31 (t, 2H, $J = 7.4$ Hz); 4.11–4.08 (t, 2H, $J = 6.4$ Hz); 2.38–2.35 (m, 2H, $J = 6.6$ Hz); 1.93–1.89 (m, 2H, $J = 7.4$ Hz); 1.32–1.20 (m, 6H); 0.80–0.76 (t, 3H, $J = 7$ Hz). ^{13}C NMR (δ_C, *ppm*, 100 *MHz*, *$CDCl_3$*): 164.4, 136.6, 134.5, 131.6, 131.5, 128.0, 127.2, 123.0, 122.7, 122.1, 50.5, 48.1, 37.0, 31.3, 30.4, 29.2, 26.0, 22.5, 14.1. IR (500–4000 cm^{-1}, KBr pellet): 2923 and 2862 (ν_{C-H}, aliphatic); 1699 ($\nu_{C=O}$); 1649 ($\nu_{C=N}$); 782 (ν_{C-H}, aromatic). TOF MS ES^+: *m*/*z* calc. for $[C_{24}H_{28}N_3O_2]^+$: 390.2182; found: 390.2190. TOF MS ES^-: *m*/*z* calc. for $[I]^-$: 126.9045; found: 126.9058. Yield: 93.32%.

SO8-I: ^{1}H NMR (δ_H, *ppm*, 400 *MHz*, *$CDCl_3$*): 9.95 (s, 1H, Ar); 8.50–8.48 (d, 2H, $J = 7.2$ Hz, Ar); 8.19–8.17 (d, 2H, $J = 8$ Hz, Ar); 7.81 (s, 1H, Ar); 7.72–7.69 (t, 2H, $J = 7.6$ Hz, Ar); 7.58 (s, 1H, Ar); 4.53–4.50 (t, 2H, $J = 6.6$ Hz); 4.40–4.37 (t, 2H, $J = 7.4$ Hz); 4.22–4.18 (t, 2H, $J = 6.4$ Hz); 2.48–2.42 (m, 2H, $J = 6.4$ Hz); 2.01–1.94 (m, 2H, $J = 7.2$ Hz); 1.39–1.25 (m, 10H); 0.86–0.83 (t, 3H, $J = 6.6$ Hz). ^{13}C NMR *(δ_C, ppm, 100 MHz, $CDCl_3$)*: 164.5, 136.7, 134.6, 131.7, 128.2, 127.2, 122.9, 122.6, 122.2, 50.7, 48.2, 37.0, 35.0, 31.9, 30.4, 29.2, 29.1, 26.4, 22.8, 14.2. IR (500–4000 cm^{-1}, KBr pellet): 3043 (ν_{C-H}, aromatic); 2929 and 2856 (ν_{C-H}, aliphatic); 1697 ($\nu_{C=O}$); 1655 ($\nu_{C=N}$); 789 (ν_{C-H}, aromatic). TOF MS ES^+: *m*/*z* calc. for $[C_{26}H_{32}N_3O_2]^+$: 418.2495; found: 418.2510. TOF MS ES^-: *m*/*z* calc. for $[I]^-$: 126.9045; found: 126.9043. Yield: 80%.

SO10-I: ^{1}H NMR *(δ_H, ppm, 400 MHz, $CDCl_3$):* 10.0 (s, 1H, Ar); 8.43–8.41 (d, 2H, $J = 6.4$ Hz, Ar); 8.13–8.10 (d, 2H, $J = 8.4$ Hz, Ar); 7.79 (s, 1H, Ar); 7.66–7.62 (t, 2H, $J = 7.8$ Hz, Ar); 7.57 (s, 1H, Ar); 4.49–4.45 (t, 2H, $J = 6.6$ Hz); 4.37–4.33 (t, 2H, $J = 7.4$ Hz); 4.15–4.12 (t, 2H, $J = 6.4$ Hz); 2.41–2.38 (m, 2H, $J = 6.6$ Hz); 1.95–1.91 (m, 2H, $J = 7.2$ Hz); 1.36–1.17 (m, 14H); 0.81–0.78 (t, 3H, $J = 7.2$ Hz). ^{13}C NMR *(δ_C, ppm, 100 MHz, $CDCl_3$):* 164.4, 136.8, 134.6, 131.7, 131.6, 128.1, 127.2, 123.0, 122.6, 122.2, 50.6, 48.2, 37.0, 32.0, 30.4, 29.6, 29.5, 29.4, 29.2, 26.4, 22.8, 14.2. IR (500–4000 cm^{-1}, KBr pellet): 2922 and 2852 (ν_{C-H}, aliphatic); 1699 ($\nu_{C=O}$); 1649 ($\nu_{C=N}$); 788 (ν_{C-H}, aromatic). TOF MS ES^+: *m*/*z* calc. for $[C_{28}H_{36}N_3O_2]^+$: 446.2808; found: 446.2823. TOF MS ES^-: *m*/*z* calc. for $[I]^-$: 126.9045; found: 126.9060. Yield: 93.45%.

2.5. Synthesis and characterization of the imidazolium bis(trifluoromethanesulfonyl) imide salts

All of the $TFSI^-$ salts were synthesized with the same reaction route. Imidazolium iodide salt (0.2 g) was added to water (40 mL) in a flask and heated to 70 °C. The mixture was left for stirring about 30 min at this temperature. Equimolar bis(trifluoromethanesulfonyl) imide salt of lithium was also dissolved in water (20 mL) and added to the stirring solution of imidazolium iodide salt. Colour of the transparent solution turned to cloudy white. The mixture left for stirring about 24 h at room temperature to proceed the ion exchange reaction and yellowish, sticky compound formed. CH_2Cl_2 was added to the mixture and imidazolium bis(trifluoromethanesulfonyl)imide salt

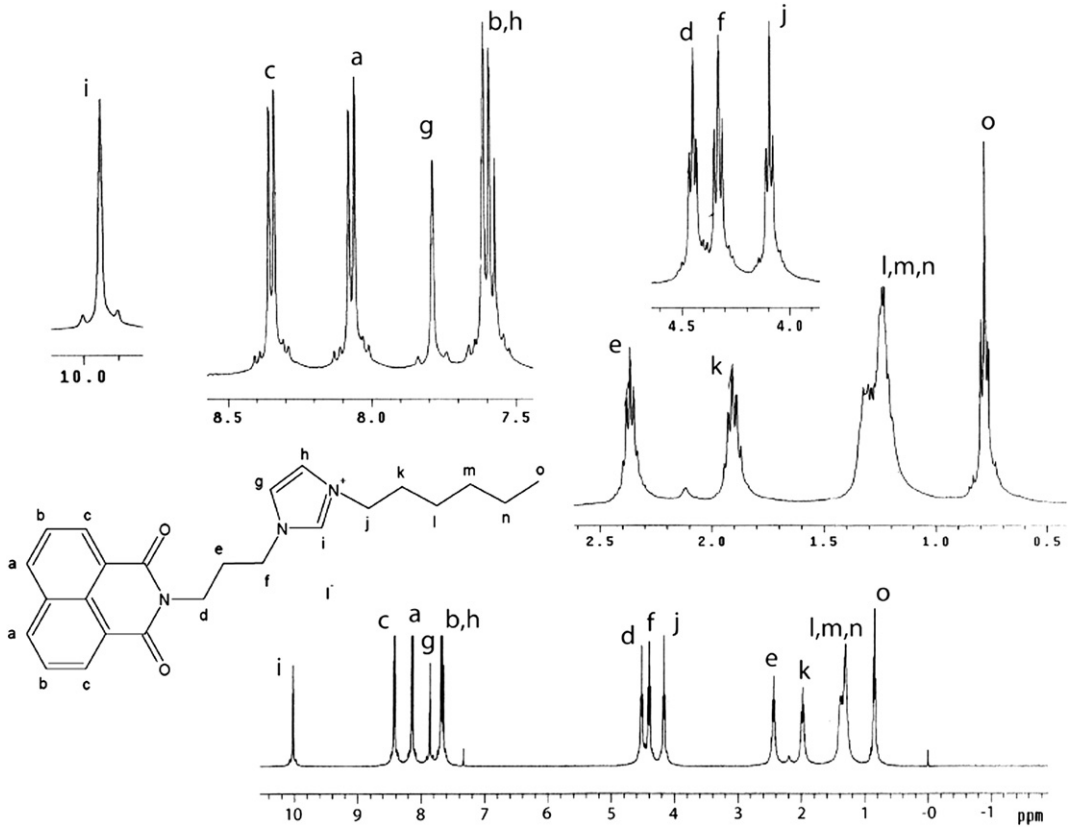

Fig. 2. ^{1}H NMR spectrum of the SO6-I salt.

extracted from the water. Then the solvent was evaporated and yellowish gel-like compound were obtained. This gel-like compound was left at room temperature and yellowish quasi-solid compound was obtained in two week by evaporation of the whole CH_2Cl_2 solvent.

SO2-TFSI: ^{1}H NMR *(δ_H, ppm, 400 MHz, DMSO):* 9.17 (s, 1H, Ar); 8.52–8.50 (d, 2H, J = 7.2 Hz, Ar); 8.50–8.47 (d, 2H, J = 8.4 Hz, Ar); 7.91–7.87 (t, 2H, J = 7.8 Hz, Ar); 7.81 (s, 1H, Ar); 7.78 (s, 1H, Ar); 4.30–4.26 (t, 2H, J = 7.4 Hz); 4.21–4.16 (q, 2H, J = 7.2 Hz); 4.14–4.11 (t, 2H, J = 6.4 Hz); 2.30–2.23 (m, 2H, J = 6.9 Hz); 1.43–1.40 (t, 3H, J = 7.2 Hz). ^{13}C NMR *(δ_C, ppm, 100 MHz, DMSO):* 164.4, 136.6, 135.1, 132.0, 131.4, 128.2, 127.9, 123.1, 122.8, 122.7, 47.7, 44.9, 37.4, 29.0, 15.63. ^{19}F-NMR *(δ_F, ppm, 376 MHz, DMSO):* −79.14 (s, $TFSI^-$) IR (500–4000 cm^{-1}, KBr pellet): 3147, 3119 (ν_{C-H} aromatic); 2994 (ν_{C-H} aliphatic); 1706 ($\nu_{C=O}$); 1663 ($\nu_{C=N}$); 1347 (ν_{SO2}); 1180 (ν_{CF3}); 1058 (ν_{SNS}). TOF MS ES$^+$: m/z calc. for $[C_{20}H_{20}N_3O_2]^+$: 334.1556; found: 334.1540. TOF MS ES$^-$: m/z calc. for $[C_2NO_4F_6S_2]^-$: 279.9173; found: 279.9167. Yield: 43.5%.

SO4-TFSI: ^{1}H NMR *(δ_H, ppm, 400 MHz, $CDCl_3$):* 8.89 (s, 1H, Ar); 8.38–8.36 (d, 2H, J = 7.6 Hz, Ar); 8.09–8.07 (d, 2H, J = 8.4 Hz, Ar); 7.63 (s, 1H, Ar); 7.63–7.59 (t, 2H, J = 7.2 Hz, Ar); 7.45 (s, 1H, Ar); 4.34–4.31 (t, 2H, J = 6.6 Hz); 4.25–4.21 (t, 2H, J = 7.4 Hz); 4.14–4.11 (t, 2H, J = 6.4 Hz); 2.38–2.34 (m, 2H, J = 6.4 Hz); 1.94–1.86 (m, 2H, J = 7.5 Hz); 1.44–1.35 (m, 2H, J = 7.4 Hz); 0.98–0.95 (t, 3H, J = 7.2 Hz). ^{13}C NMR *(δ_C, ppm 100 MHz, $CDCl_3$):* 164.5, 135.8, 134.6, 131.6, 131.4, 127.9, 127.1, 122.9, 122.8, 121.9, 50.2, 48.0, 36.8, 32.0, 29.0, 19.5, 13.4. ^{19}F-NMR *(δ_F, ppm, 376 MHz, $CDCl_3$):* −79.42 (s, $TFSI^-$). IR (500–4000 cm^{-1}, KBr pellet): 2968, 2942 (ν_{C-H} aliphatic); 1701 ($\nu_{C=O}$); 1659 ($\nu_{C=N}$); 1353 (ν_{SO2}); 1198 (ν_{CF3}); 1056 (ν_{SNS}). TOF MS ES$^+$: m/z calc. for $[C_{22}H_{24}N_3O_2]^+$: 362.1869; found: 362.1880. TOF MS ES$^-$: m/z calc. for $[C_2NO_4F_6S_2]^-$: 279.9173; found: 279.9174. Yield: 96%.

SO6-TFSI: ^{1}H NMR *(δ_H, ppm, 400 MHz, $CDCl_3$):* 8.90 (s, 1H, Ar); 8.46–8.44 (d, 2H, J = 6.4 Hz, Ar); 8.15–8.13 (d, 2H, J = 7.6 Hz, Ar); 7.69–7.65 (t, 2H, J = 7.2 Hz, Ar); 7.60 (s, 1H, Ar); 7.40 (s, 1H, Ar); 4.33–4.29 (t, 2H, J = 6.6 Hz); 4.23–4.19 (t, 2H, J = 7.4 Hz); 4.16–4.13 (t, 2H, J = 6.6 Hz); 2.39–2.32 (m, 2H, J = 6.5 Hz); 1.94–1.86 (m, 2H, J = 7.4 Hz); 1.37–1.26 (m, 6H); 0.88–0.84 (t, 3H, J = 7.2 Hz). ^{13}C NMR *(δ_C, ppm, 100 MHz, $CDCl_3$):* 164.4, 135.9, 134.6, 131.6, 131.4, 127.9, 127.1, 122.9, 122.7, 121.9, 50.4, 48.0, 36.8, 31.8, 30.2, 29.1, 26.3, 22.7, 14.1. ^{19}F-NMR *(δ_F, ppm, 376 MHz, $CDCl_3$):* −79.39 (s, $TFSI^-$). IR (500–4000 cm^{-1}, KBr pellet): 3151 (ν_{C-H} aromatic); 2964, 2864 (ν_{C-H} aliphatic); 1701 ($\nu_{C=O}$); 1659 ($\nu_{C=N}$); 1354 (ν_{SO2}); 1215 (ν_{CF3}); 1056 (ν_{SNS}). TOF MS ES$^+$: m/z calc. for $[C_{24}H_{28}N_3O_2]^+$: 390.2182; found: 390.2169. TOF MS ES$^-$: m/z calc. for $[C_2NO_4F_6S_2]^-$: 279.9173; found: 279.9177. Yield: 90%.

SO8-TFSI: ^{1}H NMR *(δ_H, ppm, 400 MHz, $CDCl_3$):* 8.91 (s, 1H, Ar); 8.42–8.40 (d, 2H, J = 6.8 Hz, Ar); 8.12–8.10 (d, 2H, J = 7.2 Hz, Ar); 7.66–7.62 (t, 2H, J = 7.6 Hz, Ar); 7.63 (s, 1H, Ar); 7.44 (s, 1H, Ar); 4.35–4.32 (t, 2H, J = 6.4 Hz); 4.24–4.21 (t, 2H, J = 7.4 Hz); 4.15–4.12 (t, 2H, J = 6.2 Hz); 2.39–2.33 (m, 2H, J = 6.3 Hz); 1.93–1.88 (m, 2H, J = 7.2 Hz); 1.34–1.24 (m, 10H); 0.86–0.82 (t, 3H, J = 6.8 Hz). ^{13}C NMR *(δ_C, ppm, 100 MHz, $CDCl_3$):* 164.7, 136.2, 134.7, 131.7, 131.7, 128.2, 127.2, 122.8, 122.5, 122.2, 50.5, 48.0, 36.8, 31.8, 30.2, 29.2, 29.05, 29.02, 26.3, 22.8, 14.2. ^{19}F-NMR *(δ_F, ppm, 376 MHz, $CDCl_3$):* −79.39 (s, $TFSI^-$). IR (500–4000 cm^{-1}, KBr pellet): 3152 (ν_{C-H} aromatic); 2926, 2859 (ν_{C-H} aliphatic); 1701 ($\nu_{C=O}$); 1659 ($\nu_{C=N}$); 1354 (ν_{SO2}); 1216 (ν_{CF3}); 1056 (ν_{SNS}). TOF MS ES$^+$: m/z calc. for $[C_{26}H_{32}N_3O_2]^+$: 418.2495; found: 418.2479. TOF MS ES$^-$: m/z calc. for $[C_2NO_4F_6S_2]^-$: 279.9173; found: 279.9167. Yield: 87.5%.

SO10-TFSI: ^{1}H NMR *(δ_H, ppm, 400 MHz, $CDCl_3$):* 8.95 (s, 1H, Ar); 8.43–8.41 (d, 2H, J = 6.4 Hz, Ar); 8.13–8.11 (d, 2H, J = 7.2 Hz, Ar); 7.66–7.62 (t, 2H, J = 8.4 Hz, Ar); 7.64 (s, 1H, Ar); 7.44 (s, 1H, Ar); 4.35–4.32 (t, 2H, J = 6.6 Hz); 4.25–4.21 (t, 2H, J = 7.4 Hz); 4.16–4.12 (t, 2H, J = 6.4 Hz); 2.38–2.35 (m, 2H, J = 6.6 Hz); 1.93–1.89 (m, 2H, J = 7 Hz); 1.34–1.22 (m, 14H); 0.86–0.82 (t, 3H, J = 6.8 Hz). ^{13}C NMR *(δ_C, ppm, 100 MHz, $CDCl_3$):* 164.5, 136.0, 134.6, 131.6, 131.5, 128.1, 127.1, 122.9, 122.7, 122.1, 50.5, 48.0, 36.8, 32.0, 30.2, 29.6, 29.5, 29.4, 29.1, 27.1, 26.3, 22.8, 14.2. ^{19}F-NMR *(δ_F, ppm, 376 MHz, $CDCl_3$):* −79.38 (s, $TFSI^-$). IR (500–4000 cm^{-1}, KBr pellet): 3151 (ν_{C-H} aromatic); 2924, 2855 (ν_{C-H} aliphatic); 1701 ($\nu_{C=O}$); 1659 ($\nu_{C=N}$); 1354 (ν_{SO2}); 1217 (ν_{CF3}); 1055 (ν_{SNS}). TOF MS ES$^+$: m/z calc. for $[C_{28}H_{36}N_3O_2]^+$: 446.2808; found: 446.2833. TOF MS ES$^-$: m/z calc. for $[C_2NO_4F_6S_2]^-$: 279.9173; found: 279.9162. Yield: 98%.

2.6. Synthesis and characterization of the imidazolium hexafluorophosphate salts

All of the PF_6^- salts were synthesized with the same reaction route. Imidazolium iodide salt (0.2 g) and slightly excess amount of NH_4PF_6 were added to MeCN solvent (20 mL) in a flask and left for stirring at room temperature for two days. After the reaction ended, MeCN was evaporated with rotary evaporator. The resultant mixture was containing desired PF_6^- salt, by-product ammonium iodide (NH_4I) and the excess of NH_4PF_6. Hexafluorophosphate salt was dissolved with CH_2Cl_2 and waste compounds were separated from the mixture by filtrating. Pure products were obtained by crystallization from the CH_2Cl_2/Diethylether (10/20 mL) mixture.

SO2-PF_6: ^{1}H NMR *(δ_H, ppm, 400 MHz, DMSO):* 9.17 (s, 1H, Ar); 8.51–8.49 (d, 2H, J = 7.2 Hz, Ar); 8.48–8.46 (d, 2H, J = 7.6 Hz, Ar); 7.91–7.87 (t, 2H, J = 7.8 Hz, Ar); 7.81 (s, 1H, Ar); 7.78 (s, 1H, Ar); 4.30–4.26 (t, 2H, J = 7.4 Hz); 4.21–4.16 (q, 2H, J = 7.2 Hz); 4.14–4.10 (t, 2H, J = 6.6 Hz); 2.30–2.23 (m, 2H, J = 7 Hz); 1.43–1.40 (t, 3H, J = 7.4 Hz). ^{31}P-NMR *(δ_P, ppm, 162 MHz, DMSO):* −130/-156 (m, PF_6^-). IR (500–4000 cm^{-1}, KBr pellet): 3167, 3120 (ν_{C-H} aromatic); 2987 (ν_{C-H} aliphatic); 1691 ($\nu_{C=O}$); 1655 ($\nu_{C=N}$); 1337 (ν_{C-N}); 838–557 (ν_{P-F}). TOF MS ES$^+$: m/z calc. for $[C_{20}H_{20}N_3O_2]^+$: 334.1556; found: 334.1476. TOF MS ES$^-$: m/z calc. for $[PF_6]^-$: 144.9642; found: 144.9637. Yield: 70%.

SO4-PF_6: ^{1}H NMR *(δ_H, ppm, 400 MHz, CD_3OD):* 9.03 (s, 1H, Ar); 8.58–8.56 (d, 2H, J = 6.4 Hz, Ar); 8.38–8.36 (d, 2H, J = 8.8 Hz, Ar); 7.85–7.81 (t, 2H, J = 7.8 Hz, Ar); 7.72–7.71 (d, 1H, J = 1.6 Hz, Ar); 7.63–7.62 (d, 1H, J = 2 Hz, Ar); 4.35–4.32 (t, 2H, J = 6.8 Hz); 4.24–4.22 (t, 2H, J = 6.4 Hz); 4.22–4.19 (t, 2H, J = 6.8 Hz); 2.42–2.35 (m, 2H, J = 6.7 Hz); 1.90–1.83 (m, 2H, J = 7.4 Hz); 1.44–1.35 (m, 2H, J = 7.6 Hz); 1.01–0.97 (t, 3H, J = 7.4 Hz). ^{31}P-NMR *(δ_P, ppm, 162 MHz, CD_3OD):* −135/−152 (m, PF_6^-). IR (500–4000 cm^{-1}, KBr pellet): 3150, 3091 (ν_{C-H} aromatic); 2960,2877 (ν_{C-H} aliphatic); 1700 ($\nu_{C=O}$); 1658 ($\nu_{C=N}$); 1349 (ν_{C-N}); 838–558 (ν_{P-F}). TOF MS ES$^+$: m/z calc. for $[C_{22}H_{24}N_3O_2]^+$: 362.1869; found: 362.1888. TOF MS ES$^-$: m/z calc. for $[PF_6]^-$: 144.9642; found: 144.9630. Yield: 55%.

SO6-PF_6: ^{1}H NMR *(δ_H, ppm, 400 MHz, $CDCl_3$):* 8.91 (s, 1H, Ar); 8.59–8.57 (d, 2H, J = 6 Hz, Ar); 8.24–8.22 (d, 2H, J = 6.8 Hz, Ar); 7.78–7.74 (t, 2H, J = 7.8 Hz, Ar); 7.56 (s, 1H, Ar); 7.28 (s, 1H, Ar); 4.33–4.30 (t, 2H, J = 6.4 Hz); 4.25–4.21 (t, 2H, J = 7.2 Hz); 4.23–4.19 (t, 2H, J = 6.4 Hz); 2.42–2.36 (m, 2H, J = 6.4 Hz); 1.97–1.90 (m, 2H, J = 7 Hz); 1.37–1.32 (m, 6H); 0.91–0.87 (t, 3H, J = 7 Hz). ^{31}P-NMR *(δ_P, ppm, 162 MHz, $CDCl_3$):* −134/−152 (m, PF_6^-). IR (500–4000 cm^{-1}, KBr pellet): 3154, 3092 (ν_{C-H} aromatic); 2956,2931,2868 (ν_{C-H} aliphatic); 1698 ($\nu_{C=O}$); 1659 ($\nu_{C=N}$); 1345 (ν_{C-N}); 837–558 (ν_{P-F}). TOF MS ES$^+$: m/z calc. for $[C_{24}H_{28}N_3O_2]^+$: 390.2182; found: 390.2210. TOF MS ES$^-$: m/z calc. for $[PF_6]^-$: 144.9642; found: 144.9636. Yield: 78.7%.

SO8-PF_6: ^{1}H NMR *(δ_H, ppm, 400 MHz, DMSO):* 9.17 (s, 1H, Ar); 8.52–8.50 (d, 2H, J = 8 Hz, Ar); 8.50–8.48 (d, 2H, J = 8.8 Hz, Ar); 7.91–7.88 (t, 2H, J = 8.8 Hz, Ar); 7.82 (s, 1H, Ar); 7.78 (s, 1H, Ar); 4.31–4.27 (t, 2H); 4.16–4.13 (t, 2H, J = 7.2 Hz); 4.13–4.09 (t, 2H, J = 6.4 Hz); 2.29–2.22 (m, 2H, J = 6.8 Hz); 1.81–1.76 (m, 2H, J = 6.9 Hz); 1.26–1.24 (m, 10H); 0.85–0.81 (t, 3H, J = 7 Hz). ^{31}P-NMR *(δ_P, ppm, 162 MHz, DMSO):* −130/-156 (m, PF_6^-). IR (500–4000 cm^{-1}, KBr pellet): 3154 (ν_{C-H} aromatic); 2928,2858 (ν_{C-H} aliphatic); 1695 ($\nu_{C=O}$); 1658 ($\nu_{C=N}$); 1336 (ν_{C-N}); 837–557 (ν_{P-F}). TOF MS ES$^+$: m/z calc. for $[C_{26}H_{32}N_3O_2]^+$: 418.2495; found: 418.2547. TOF MS ES$^-$: m/z calc. for $[PF_6]^-$: 144.9642; found: 144.9645. Yield: 64%.

SO10-PF_6: ^{1}H NMR (δ_H, *ppm, 400 MHz, $CDCl_3$):* 8.76 (s, 1H, Ar); 8.46–8.44 (d, 2H, J = 7.6 Hz, Ar); 8.12–8.10 (d, 2H, J = 8 Hz, Ar) 7.68–7.64 (t, 2H, J = 8 Hz, Ar); 7.57 (s, 1H, Ar); 7.34 (s, 1H, Ar); 4.32–4.29 (t, 2H, J = 6.8 Hz); 4.22–4.18 (t, 2H, J = 7.8 Hz); 4.15–4.11 (t, 2H, J = 6.2 Hz); 2.38–2.31 (m, 2H, J = 6.4 Hz); 1.94–1.87 (m, 2H, J = 7.2 Hz); 1.34–1.22 (m, 14H); 0.86–0.82 (t, 3H, J = 6.8 Hz). ^{31}P-NMR (δ_P, *ppm, 162 MHz, $CDCl_3$):* −134/−152 (m, PF_6^-). IR (500–4000 cm^{-1}, KBr pellet): 2927, 2856 (ν_{C-H} aliphatic); 1701 ($\nu_{C=O}$); 1657 ($\nu_{C=N}$); 1344 (ν_{C-N}); 838–558 (ν_{P-F}). TOF MS ES$^+$: m/z calc. for $[C_{28}H_{36}N_3O_2]^+$: 446.2808; found: 446.2844. TOF MS ES$^-$: m/z calc. for $[PF_6]^-$: 144.9642; found: 144.9620. Yield: 53.4%.

3. Result and discussion

3.1. Spectrophotometric studies

3.1.1. UV–Vis absorption and fluorescence properties

UV–Vis absorption spectra of the imidazolium salts have shown two absorption bands in $CHCl_3$. Absorption maxima and corresponding molar extinction constants ($\acute{a}$) are given in Table 2. Alternation of the anion or alkyl chain did not change the maximum absorption wavelengths of the compounds. All compounds have maximum absorption wavelengths at about 337 nm and 351 nm, originating from the π–π* transitions of the 1,8-naphthalimide groups. It is indicated in literature that the lowest excited state is predominantly in π–π* character for 1,8-naphthalimides and fast intersystem crossing (ISC) from the excited π–π* singlet state to a close-lying n–π* triplet state is particularly efficient in the case of the 1,8-naphthalimides [39].

Fluorescence quantum yields were calculated with reference to the absorption and fluorescence emission spectra of anthracene in EtOH (Φ_f = 0.27) [40,41].

Absorbance values of the solutions at the excitation wavelength were smaller than 0.2 to prevent the concentration quenching. The calculated Φ_f values were corrected for the index of refraction differences. Indexes of refraction were taken as 1.47 and 1.36 for $CHCl_3$ and EtOH, respectively. All of the excitations were carried out at the wavelength that is abbreviated as $\ddot{e}_1$ in Table 2. The equation used in calculation of fluorescence quantum yield is given in Eq. (1):

$$\Phi_f = \Phi_{fs} x \frac{S_u}{S_s} x \frac{A_s}{A_u} x \frac{n_u^2}{n_s^2} \quad (1)$$

Table 2
Absorption and fluorescence properties of the synthesized salts [absorption wavelength, λ (nm); molar extinction coefficient, ε x 10^{-4} (M^{-1} cm^{-1}); excitation wavelength, λ* (nm); emission wavelength, λ_{em} (nm); fluorescence quantum yield, Φ_f; radiative lifetime, τ_0 x 10^{11} (s); quenching rate constant, k_q x 10^{-14} (M^{-1} s^{-1})] and Gibbs free energy, ΔG_{ET} (kcal mol^{-1})].

Compound	λ_1^*	ε_1	λ_2	ε_2	λ_{em}	Φ_f	τ_0	k_q	ΔG_{ET}
SO	337	1.4	351	1.3	370, 385	0.0310	0.10	1.8	–
SO2-I	338	1.6	352	1.5	369, 384	0.0085	9.28	1.8	−33.43
SO4-I	338	1.0	351	0.9	370, 386	0.0088	13.7	2.3	−32.04
SO6-I	338	0.9	353	0.9	370, 386	0.0112	15.1	3.0	−32.27
SO8-I	337	1.7	353	1.6	371, 387	0.0112	8.22	4.2	−33.68
SO10-I	337	1.7	353	1.8	370, 386	0.0123	8.37	4.6	−32.52
SO2-TFSI	338	1.4	353	1.2	370, 386	0.1629	12.0	2.2	−26.50
SO4-TFSI	338	1.4	352	1.2	370, 386	0.1675	12.6	2.2	−26.74
SO6-TFSI	338	1.5	353	1.3	369, 386	0.1558	10.2	3.2	−29.97
SO8-TFSI	338	1.5	352	1.3	371, 386	0.1611	11.7	2.7	−30.89
SO10-TFSI	338	1.6	353	1.4	370, 386	0.1570	9.8	3.1	−30.20
SO2-PF_6	337	2.0	353	1.8	368, 386	0.1608	6.84	2.6	−18.23
SO4-PF_6	338	2.2	353	1.9	369, 386	0.1771	6.16	2.4	−20.74
SO6-PF_6	338	2.4	353	2.1	370, 386	0.1905	5.73	2.6	−19.13
SO8-PF_6	338	1.7	353	1.6	368, 386	0.1774	8.03	2.0	−19.36
SO10-PF_6	338	1.4	353	1.2	368, 386	0.1856	9.63	1.9	−17.52

where, Φ_f is the fluorescence quantum yield, A is the absorption intensity, S is the integrated emission band area and n is the solvent reflective index, u and s refer to the unknown and standard, respectively.

The fluorescence quantum yields of the synthesized compounds were very low, because of the fast ISC property of the unsubstituted 1,8-naphthalimide groups [42]. The Φ_f value of the unsubstituted 1,8-naphthalimide was determined as 0.029 in the literature and that of SO, in this study, is calculated as 0.031. This slight increase in the Φ_f may indicate the donor and acceptor relation between the imidazole and the 1,8-naphthalimide group, respectively.

Iodide salts have very low Φ_f values with regard to the starting material, *i.e.* SO. This decrease can be explained by the heavy atom effect of the iodide ions [43]. Heavy atoms like iodide or bromide increase the spin-orbit coupling and therefore increase the $S_1 \rightarrow T_1$ (ISC) transitions. Increased $S_1 \rightarrow T_1$ transitions reduce the fluorescence emission and accordingly the fluorescence quantum yield. In the case of PF_6^- and $TFSI^-$ anions, higher Φ_f values ($\Phi_f \cong 0.2$) were obtained. These higher Φ_f values may be attributed to the increased electron donating property of the $TFSI^-$ and PF_6^- ions to the 1,8-naphthalimide group.

3.1.2. Fluorescence quenching studies

The quenching of fluorescence emission for I^- and $TFSI^-$ salts were studied with cis-bis(isothiocyanato) (2,2′-bipyridyl-4,4′-dicarboxylato) (2,2′-bipyridyl-4,4′-di-nonyl) ruthenium(II), i.e. Z907, since these salts were planned to use as electrolyte components in DSSCs. Quenching studies of PF_6^- salts were performed with tris(8-hydroxyquinoline)aluminum (Alq_3) since these salts were synthesized for OLED applications. Molecular structures of the Z907 dye and the Alq_3 are shown in Fig. 3.

1×10^{-5} M solutions of the synthesized salts and 1×10^{-3} M solutions of Z907/Alq_3 were prepared in $CHCl_3$. 10–20 μL Z907/Alq_3 solutions were added to the solutions of the salts and the fluorescence intensities were recorded. The fluorescence quenching rate constants (k_q, M^{-1} s^{-1}) were calculated from the Stern–Volmer equation (2) [44]:

$$I_0/I = 1 + k_q \tau_0 [Q] \quad (2)$$

where I_0 and I represent the fluorescence intensity of imidazolium salts in the absence and presence of quencher respectively. [Q] is the concentration of the quencher (M) and τ_0 is the radiative lifetime (s) in the absence of the quencher. τ_0 values were calculated by the use of Eq. (3):

$$\tau_0 = \frac{3.5x10^8}{\upsilon_{max}^2 \varepsilon_{max} \Delta\upsilon_{1/2}} \quad (3)$$

where υ_{max} is the wave number per centimeter (cm^{-1}), ε_{max} is the molar extinction coefficient at the selected absorption wavelength (M^{-1} cm^{-1}) and $\Delta\upsilon_{1/2}$ is the half width of the selected absorption wave number (cm^{-1}) where the excitation was performed.

Fluorescence quenching of I^-, $TFSI^-$ and PF_6^- salts were studied at increasing concentration of Z907 and Alq_3. High k_q values of $\sim 10^{14}$ can be attributed to efficient electron transfer process from these salts to Z907 and Alq_3. These quenching studies show that I^- and $TFSI^-$ salts may be appropriate compounds for DSSC applications as electrolyte and PF_6^- salts may be used as additives and/or electron transport materials in OLEDs. Fluorescence quenching spectra and Stern–Volmer plots of SO6-I, SO6-TFSI and SO6-PF_6 are shown in Figs. 4 and 5, respectively. The intensity increase observed in Fig. 5 is due to the increasing emission of Alq_3 (the quencher) with its concentration in SO6-PF_6 salt solution. This increase is present, unexceptionally, in all quenching studies performed between PF_6^- salts and Alq_3.

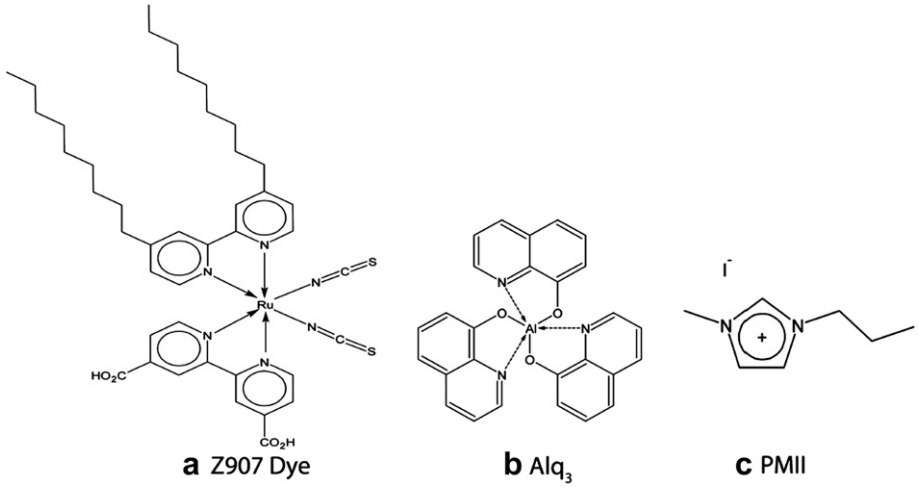

Fig. 3. Molecular structures of a) Z907 dye, b) Alq_3 and c) PMII.

Quenching data can be analyzed by using the Weller equation (4); which is used to calculate the free energy in quenching by electron transfer when the excited-state energy of the excited reactant and redox potentials of both reactants are known [45],

$$\Delta G_{ET}(\text{kcal mol}^{-1}) = 23.06\left[E(D^*/D) - E(A/A^-)\right] - E_D^* \quad (4)$$

This equation is used to determine whether electron transfer between an excited state and ground state is spontaneous. The calculated ΔG_{ET} values were all lower than −5 kcal mol^{-1} (the "rule of thumb" [46]) and may account for a favorable electron transfer between the imidazolium salts and the quenchers. The fact that all of the iodide salts almost have the same free energy of electron transfer indicates that alkyl chain length does not have a considerable effect on the electron transfer. This situation is valid for the $TFSI^-$ and PF_6^- salts as well. Computed free energies are also provided in Table 2 and they support high k_q values of around 10^{14} M^{-1} s^{-1}.

3.1.3. Photostability studies

As far as we know photostability studies of the ionic liquids have not been studied yet. Photostability of the compounds come into prominence in long term applications. Especially for DSSC applications, photostability of cell components is very important. The equation used in photostability studies is given below (Eq. (5)),

$$-\ln\left(\frac{I_0}{I}\right) = k_p t \quad (5)$$

where I_0 and I are the emission intensity of the compound at times zero and t, k_p the first-order rate constant (s^{-1}). Half-lives $t_{1/2}$ (s) were calculated using Eq. (6) which was derived from Eq. (5) by placing I with $I/2$.

$$t_{1/2} = -\frac{\ln(1/2)}{k_p} = \frac{0.693}{k_p} \quad (6)$$

Photostability experiments of I^-, $TFSI^-$ and PF_6^- salts in solution of $CHCl_3$ were performed on exposure to xenon lamp of a fluorescence spectrophotometer. The data were acquired at 338 nm for the duration of 60 min. This wavelength corresponds to the emission maxima of studied imidazolium salts in $CHCl_3$. The emission intensity of I^- salts gave an upward intensity. Therefore, the obtained data were analyzed only for $TFSI^-$ and PF_6^- salts. The photostability study of PMII was also performed for comparison, since it is one of the most common and efficient ionic liquid used in DSSC applications. The molecular structure of PMII is shown in Fig. 3. According to the emission spectra analysis, photostabilities of the synthesized compounds were quiet high compared to the standard PMII and half-lives change between 19 and 48 h. Results are shown in Table 3.

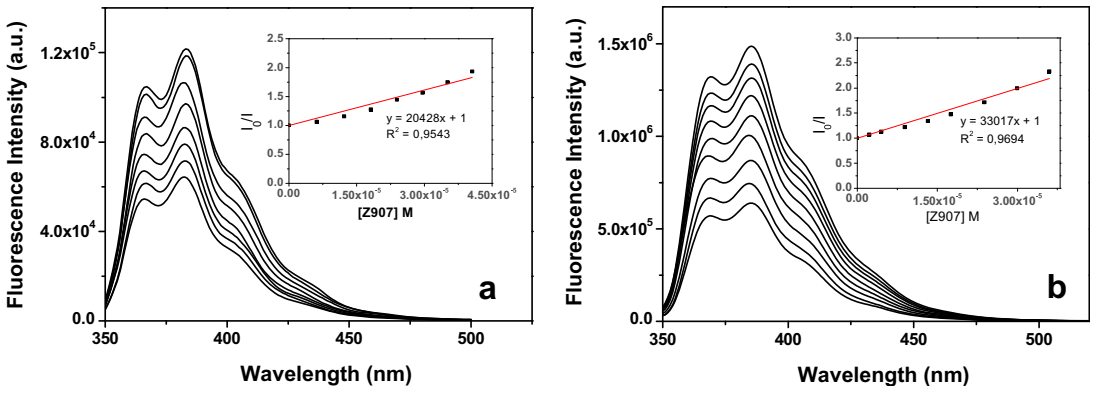

Fig. 4. Fluorescence emission quenching of (a) SO6-I, (b) SO6-TFSI with increasing Z907 concentration in $CHCl_3$ solution and the insets are the corresponding Stern–Volmer plots. (The fluorescence located at 350–450 nm belongs to the naphthalimide group of the synthesized compounds).

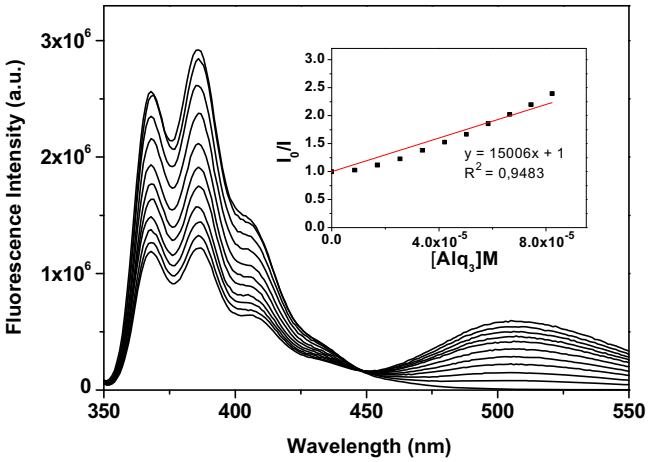

Fig. 5. Fluorescence emission quenching of SO6-PF_6, with increasing Alq_3 concentration in $CHCl_3$ solution and inset is the corresponding Stern–Volmer plot. (The fluorescence located at 450–550 nm belongs to the Alq_3).

The amphiphilic heteroleptic ruthenium complexes (e.g. Z907) represent one of the widely studied groups of dyes in DSSCs [47–49]. Photostability of dye and other cell components is one of the limiting factors effecting the DSSC lifetime. Ocakoglu et al. have reported that depending on the solvent used, the $t_{1/2}$ values of ruthenium complexes changes between 3.85 and 19.25 h [50]. The highest $t_{1/2}$ value reported is equal to the lowest $t_{1/2}$ value calculated for $TFSI^-$ salts. That supports and strengthens the possibility of $TFSI^-$ salts to be efficient electrolytes in DSSC systems. The photostability of PF_6^- salts was either equal to or higher than that of the $TFSI^-$ salts with the same alkyl chain length. The alkyl chain length seems to have an impact on the $t_{1/2}$ values. The optimized alkyl chain length can be reported as six, as the minimum k_p values are obtained for them. The differences in three dimensional geometry of the alkyl substituents of the synthesized molecules at the excited state may have an influence on this result.

3.2. Electrochemical behavior

The electrochemical stability of the synthesized compounds was determined from their cyclic voltammograms. All solutions were purged with nitrogen before starting the measurements. The electrochemical studies were performed in a cell containing Ag wire reference electrode, glassy carbon working electrode, Pt wire counter electrode and 0.1 M TBAPF6 in MeCN. Ferrocene was employed as a standard in these measurements [$E^\circ(Fc/Fc^+) = 0.47$ V vs. Ag in MeCN]. Scan rate was kept as 0.2 V s^{-1} for all compounds. The onset potentials of the first reduction peaks were used to determine the lowest unoccupied molecular orbital (LUMO) energy levels depending on the value of 4.8 eV for ferrocene with respect to vacuum level and by the use of following equation (7) [51]

$$E_{LUMO} = -e\left(E_{1/2(red,\ dye)} - E_{1/2(Fc)} + 4.8\right) \quad (7)$$

Table 4
Electrochemical properties and conductivity values of synthesized compounds.

Compound	$E_{1/2(ox)_1}$(V)	$E_{1/2(ox)_2}$ (V)	$E_{1/2(red)}$(V)	E_{LUMO} (eV)	E_g (Optical)	σ(S/cm)
SO	–	–	−1.39	−3.01	3.40	–
SO2-I	0.91	1.10	−0.91	−3.42	3.39	0.137
SO4-I	0.97	1.15	−0.91	−3.42	3.40	0.145
SO6-I	0.96	1.14	−0.90	−3.43	3.38	0.916
SO8-I	0.91	1.11	−0.92	−3.41	3.40	0.021
SO10-I	0.96	1.13	−0.90	−3.43	3.39	0.004
SO2-TFSI	–	–	−1.21	−3.11	3.40	0.005
SO4-TFSI	–	–	−1.20	−3.12	3.39	0.008
SO6-TFSI	–	–	−1.06	−3.26	3.39	0.013
SO8-TFSI	–	–	−1.02	−3.30	3.39	0.006
SO10-TFSI	–	–	−1.05	−3.27	3.40	0.005
SO2-PF_6	–	–	−1.19	−3.13	3.40	0.025
SO4-PF_6	–	–	−1.07	−3.25	3.39	0.037
SO6-PF_6	–	–	−1.14	−3.18	3.39	0.039
SO8-PF_6	–	–	−1.13	−3.19	3.39	0.009
SO10-PF_6	–	–	−1.21	−3.11	3.40	0.008

The redox potentials, LUMO energy levels and optical band gaps are summarized in Table 4.

It is accepted that reduction peaks of the ionic liquids are originated from decomposition of the cation and oxidation peaks arise from decomposition of the anion. In the imidazolium ILs, it is assumed that reduction peaks are originated from reduction of acidic C_2 proton of the imidazolium cation [52]. The cathodic reaction starts at or below −2.5 V for imidazolium salts with $TFSI^-$, PF_6^- and BF_4^- anions [53,54]. In our study, all synthesized compounds show a reversible reduction peak originated from the electron-deficient naphthalimide groups. The reduction of the acidic C_2 proton of the imidazolium cation has not been observed in the studied region (2 V/-2 V).

Kolthoff and Coetzee [55] have reported that electro-oxidation of iodide ion in acetonitrile comprises two oxidation waves. The first involves oxidation of iodide ion to triiodide ion and the second involves oxidation of triiodide ion to iodine. This process can be shown as;

$$6I^- = 2I_3^- + 4e$$
$$2I_3^- = 3I_2 + 2e$$

In this study the synthesized imidazolium iodide salts also have two anodic peaks which belong to oxidation of the iodide ions by two steps. However, PF_6^- and $TFSI^-$ salts didn't show any oxidation peak until 2 V potential. These results are well matched with the studies of Yeon et al. [54]. They have investigated the electrochemical properties of some imidazolium ILs and indicate that PF_6^-, BF_4^- and $TFSI^-$ salts of the same imidazolium cation did not show any oxidation peak until 3 V potential. Cyclic voltammograms of imidazolium cation, SO10, with different anions are shown in Fig. 6.

3.3. Thermal analysis

Melting points and thermal degradation temperatures of the synthesized salts were determined from the DSC and TGA measurements, respectively. The flow rate of nitrogen was 20 mL min^{-1} and

Table 3
Rate constants (k_p, s^{-1}) and half-lives ($t_{1/2}$) for photodegradation of PMII, PF_6^- and $TFSI^-$ salts ($t_{1/2}$ values obtained in seconds were converted into hours).

	$PMII^-$	$TFSI^-$					PF_6^-				
		SO2	SO4	SO6	SO8	SO10	SO2	SO4	SO6	SO8	SO10
$k_p \times 10^5$	5	1.0	1.0	0.4	0.6	0.4	1.0	0.7	0.4	1.0	1.0
$t_{1/2}$ (h)	3.85	19.25	19.25	48.12	32.08	48.12	19.25	27.50	48.12	19.25	19.25

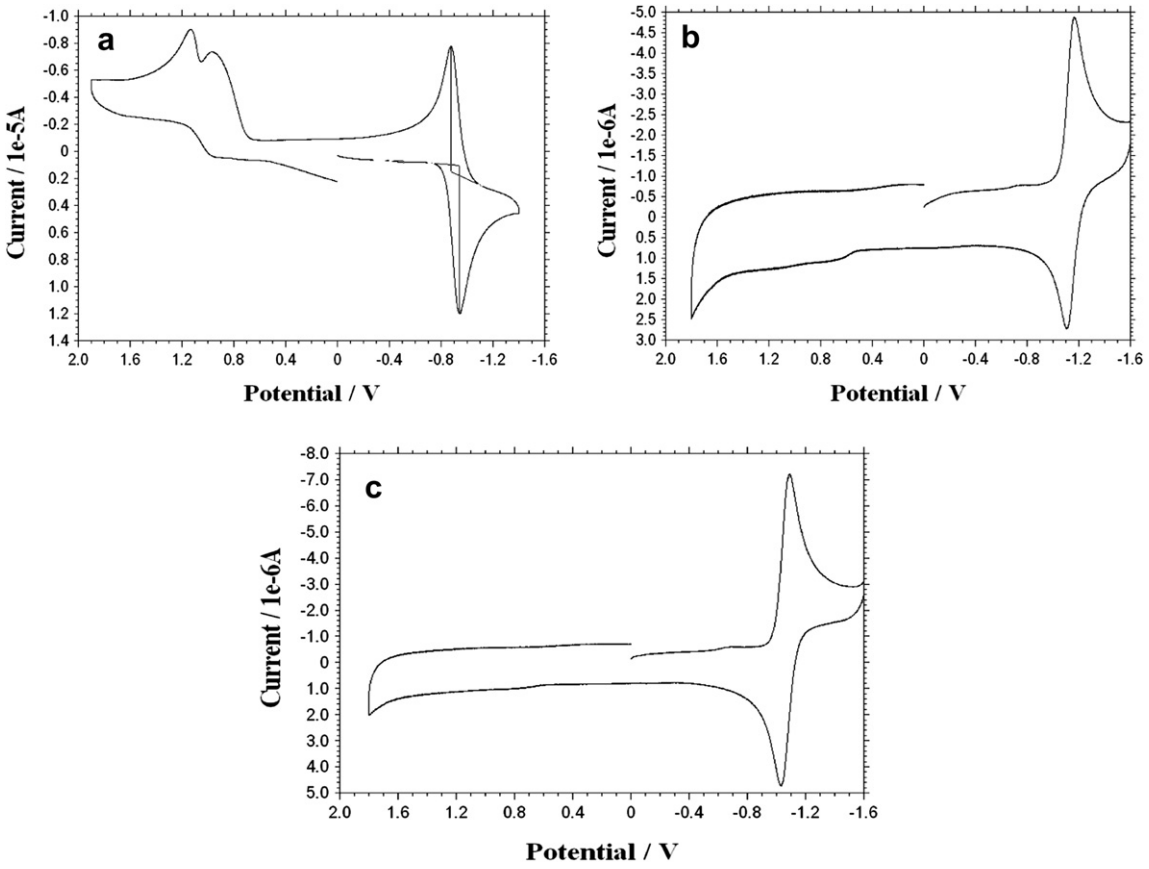

Fig. 6. Cyclic voltammograph of SO6-I (a), SO6-PF_6 (b) and SO6-TFSI (c).

the constant heating rate was 20 °C min^{-1} for both DSC and TGA measurements. Sealed and unsealed alumina pans were used for DSC and TGA measurements, respectively. DSC and TGA curves of some imidazolium salts are given in Figs. 7 and 8.

By increasing the alkyl chain length, the melting points of imidazolium iodide salts changed from 196 °C to 106 °C and generally decreased by increasing the alkyl chain length. The trend of melting point depression is in good agreement with the studies of Ngo et al. [56]. They have investigated the properties of a series of imidazolium ILs and pointed out that larger more asymmetrical cations cause lower melting points. Alkyl chain lengthening may cause the disruption of the symmetry and lead to lower melting points.

The melting points of PF_6^- salts with regard to the alkyl chain length were not ordered. SO2-PF_6, SO6-PF_6 and SO8-PF_6 have higher melting points according to corresponding iodide salt, SO4-PF_6, SO10-PF_6 have lower melting points as compared to the corresponding iodide salt. Melting points of the TFSI salts decreased dramatically compared to the other salts. The lower melting points of these salts are probably related to their inability to form H-bonds and better charge delocalization of the $TFSI^-$ anion [52]. In the next

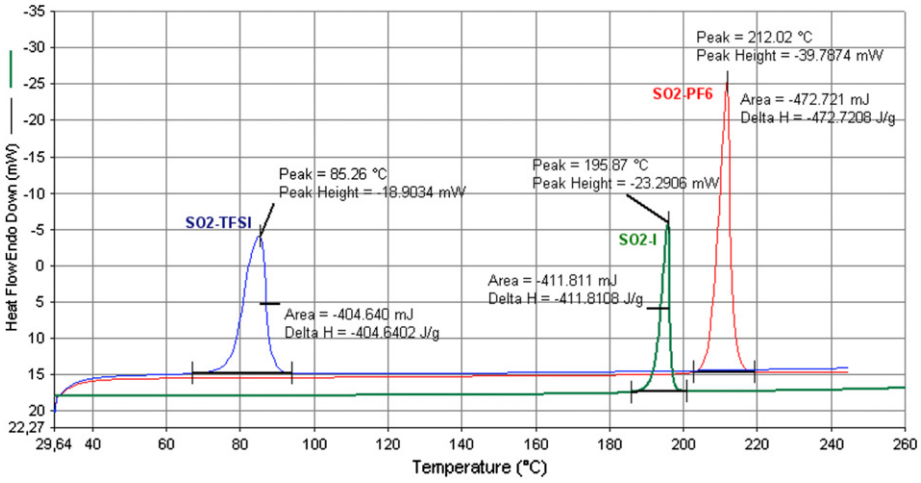

Fig. 7. DSC scans for SO2-TFSI, SO2-I and SO2-PF_6, showing distinct melting points of the compounds.

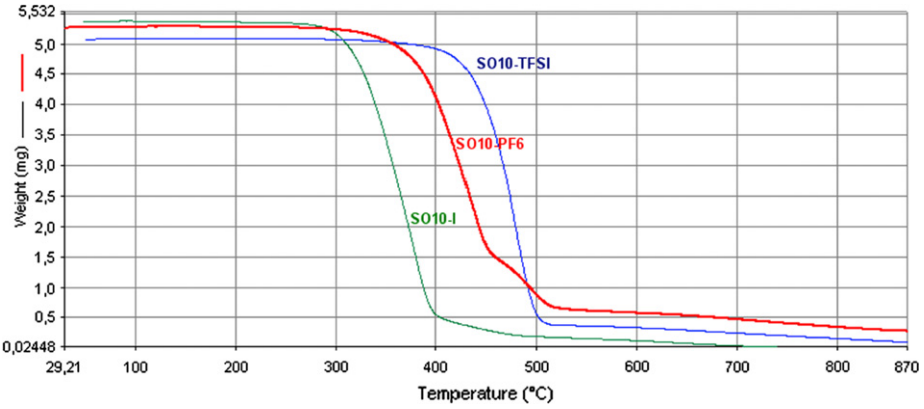

Fig. 8. Characteristic decomposition curves of SO10-I, SO10-PF_6 and SO10-TFSI determined by TGA measurements.

studies, XRD analyses will be performed to understand the effect of the molecular interactions on the melting points.

The vast majority of the ILs have a high thermal stability usually up to 400 °C. Kosmulski et al. indicated that thermal stability of an IL depends on the anion and the effect of the cation is rather insignificant [57]. Also it is reported that, thermal stability increases with increasing anion size [58] and decreases with its hydrophilicity [59]. Fox et al. have pointed out that nucleophilic anions reduce the thermal stability compared to bulky fluoride containing anions and the alkyl chain length does not have a large effect on the thermal stability [60]. In accordance with these explanations, there is not a significant correlation in the thermal stabilities of the synthesized compounds with respect to the alkyl chain length. However, it is obvious that the anion has an important effect on the thermal stabilities. Imidazolium salts with the hydrophilic iodide anions have lower degradation temperatures compared to the salts with hydrophobic anions. The thermal stabilities of the iodide salts change between 378 and 381 °C independent from the alkyl chain length on the imidazole group (Table 5). Synthesized PF_6^- salts have higher degradation temperatures than the iodide salts and change between 409 and 431 °C. Kroon et al. [61] have investigated the degradation mechanisms of some ILs via quantum chemical calculations and indicate that $TFSI^-$ anion is more thermally stable than PF_6^- anion. They also suggest that nucleophilic and highly proton-abstracting halide anions decompose at much lower temperatures compared to poorly proton-abstracting anions, such the $TFSI^-$ anion. In a good agreement with these studies, $TFSI^-$ salts are the most thermally stable compounds among synthesized imidazolium salts and their stabilities approach to 500 °C.

Table 5
Thermal analysis results of the compounds.

Cations	I^-		$PF6^-$		$TFSI^-$	
	T_m (°C)	T_d (°C)	T_m (°C)	T_d (°C)	T_m (°C)	T_d (°C)
SO2	196	381	212	426	85	498
SO4	174	383	140	431	50	453
SO6	127	384	135	409	74	484
SO8	105	385	145	411	73	470
SO10	106	378	91	441	78	475

T_m: Temperature of the melting point, T_d: Temperature of the thermal degradation.

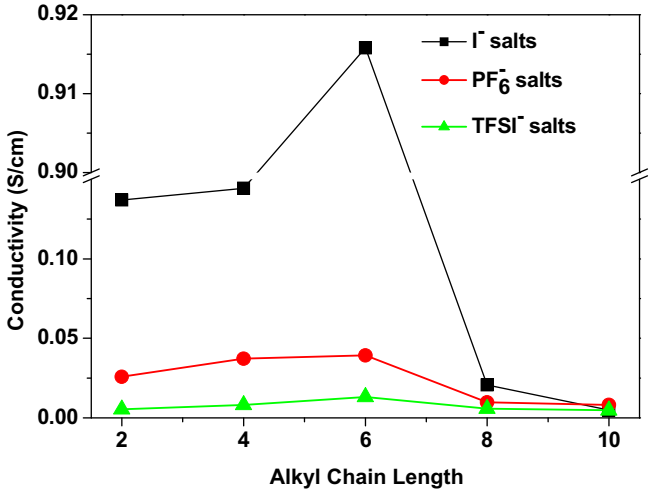

Fig. 9. Conductivity versus alkyl chain length of napthalimide imidazolium salts.

3.4. Conductivity

The conductivity (σ) characteristics of the synthesized compounds were measured in a sandwich structure, according to the literature procedure [62]. Al was vacuum evaporated on glass substrate and the compounds were spin coated from their concentrated solutions in DMF over the Al coatings. Six Al contacts having the active area of 0.16 cm^2 each, were deposited on the upper surface of the film. The σ values were determined from the current-voltage characteristics of the films. Conductivities of all naphthalimide imidazolium salts were increased up to a maximum value for six carbon alkyl chain length and then decreased with a further increase of alkyl chain length (Table 4 and Fig. 9).Additionally, the σ values were decreased with the increased ion size from I^- to $TFSI^-$ which is in a good agreement with the literature [63].

4. Conclusion

In conclusion, 1,8-naphthalimides with tethered imidazolium salts were synthesized, and their photophysical, electrochemical and thermal properties have been studied. Quenching studies and Gibbs free energy calculations have been performed. High quenching rate constant and low Gibbs free energy values indicate an efficient electron transfer from I^- and $TFSI^-$ salts to Z907 dye and from PF_6^- salts to Alq_3 material. The synthesized compounds showed high photostability and high thermal stability that promote their usability in various applications. Hence, I^- and $TFSI^-$ salts can be use as electrolyte components for DSSC's and PF_6^- salt can be use in OLED applications. Their further studies of interesting applications will be done in the near future.

Acknowledgments

We thank to Dr. Nimal Gunaratne and Prof. Dr. K. R. Seddon from QUILL Research Center for the electrospray mass measurements. We acknowledge the project support funds of Ege University and State Planning Organization of Turkey (DPT).

References

[1] Hagiwara R, Ito Y. Room temperature ionic liquids of alkylimidazolium cations and fluoroanions. J Fluor Chem 2000;105(2):221–7.
[2] Huddleston JG, Visser AE, Reichert WM, Willauer HD, Broker GA, Rogers RD. Characterization and comparison of hydrophilic and hydrophobic room temperature ionic liquids incorporating the imidazolium cation. Green Chem 2001;3:156–64.
[3] Buzzeo MC, Evans RG, Compton RG. Non-haloaluminate room-temperature ionic liquids in electrochemistry – a review. Chem Phys Chem 2004;5(8):1106–20.
[4] Ohno H, editor. Electrochemical aspects of ionic liquids. John Wiley and Sons, Inc.; 2005. p. 173–223.
[5] Fernicola A, Scrosati B, Ohno H. Potentialities of ionic liquids as new electrolyte media in advanced electrochemical devices. Ionics 2006;12(2):95–102.
[6] Galinski M, Lewandowski A, Stepniak I. Ionic liquids as electrolytes. Electrochim Acta 2006;51(26):5567–80.
[7] Anderson JL, Ding J, Welton T, Armstrong DW. Characterizing ionic liquids on the basis of multiple solvation interactions. J Am Chem Soc 2002;124(47):14247–54.
[8] Dzyuba SV, Bartsch RA. Expanding the polarity range of ionic liquids. Tetrahedron Lett 2002;43(26):4657–9.
[9] Znamenskiy V, Kobrak MN. Molecular dynamics study of polarity in room-temperature ionic liquids. J Phys Chem B 2004;108(3):1072–9.
[10] Aki SNVK, Brennecke JF, Samanta A. How polar are room-temperature ionic liquids? Chem Commun; 2001:413–4.
[11] Carmichael AJ, Seddon KR. Polarity study of some 1-alkyl-3-methylimidazolium ambient-temperature ionic liquids with the solvatochromic dye, Nile Red. J Phys Org Chem 2000;13(10):591–5.
[12] Yeon S-H, Kim K-S, Choi S, Cha J-H, Lee H. Characterization of PVdF(HFP) gel electrolytes based on 1-(2-hydroxyethyl)-3-methyl imidazolium ionic liquids. J Phys Chem B 2005;109(38):17928–35.
[13] Kubo W, Kitamura T, Hanabusa K, Wada Y, Yanagida S. Quasi-solid-state dye-sensitized solar cells using room temperature molten salts and a low molecular weight gelator. Chem Commun; 2002:374–5.
[14] Wang P, Zakeeruddin SM, Moser J-E, Gratzel M. A new ionic liquid electrolyte enhances the conversion efficiency of dye-sensitized solar cells. J Phys Chem B 2003;107(48):13280–5.
[15] Murai S, Mikushiba S, Sumina H, Kato T, Hayase S. Quasi-solid dye sensitised solar cells filled with phase-separated chemically cross-linked ionic gels. Chem Commun; 2003:1534–5.
[16] Kubo W, Kambe S, Nakade S, Kitamura T, Hanabusa K, Wada Y, et al. Photocurrent-determining processes in quasi-solid-state dye-sensitized solar cells using ionic gel electrolytes. J Phys Chem B 2003;107(18):4374–81.
[17] Wang P, Zakeeruddin SM, Baker RH, Gratzel M. A binary ionic liquid electrolyte to achieve $\geq$7% power conversion efficiencies in dye-sensitized solar cells. Chem Mater 2004;16(14):2694–6.
[18] Martin R, Teruel L, Aprile C, Cabeza JF, Alvaro M, Garcia H. Imidazolium ionic liquids in OLEDs: synthesis and improved electroluminescence of an 'ionophilic' diphenylanthracene. Tetrahedron 2008;64(27):6270–4.
[19] Yap CC, Yahaya M, Salleh MM. Influence of thickness of functional layer on performance of organic salt-doped OLED with ITO/PVK: PBD:TBAPF6/Al structure. Curr Appl Phys 2008;8(5):637–44.
[20] Lee J, Panzer MJ, He Y, Lodge TP, Frisbie CD. Ion gel gated polymer thin-film transistors. J Am Chem Soc 2007;129(15):4532–3.
[21] Ue M, Takeda M, Takahashi T, Takehara M. Ionic liquids with low melting points and their application to double-layer capacitor electrolytes. Electrochem Solid State Lett 2002;5(6):A119–21 [makale yok].
[22] Balducci A, Bardi U, Caporali S, Mastragostino M, Soavi F. Ionic liquids for hybrid supercapacitors. Electrochem Commun 2004;6(6):566–70.
[23] Sato T, Masuda G, Takagi K. Electrochemical properties of novel ionic liquids for electric double layer capacitor applications. Electrochim Acta 2004;49(21):3603–11.
[24] De Souza RF, Padilha JC, Gonçalves RS, Dupont J. Room temperature dialkylimidazolium ionic liquid-based fuel cells. Electrochem Commun 2003;5(8):728–31.
[25] Garcia B, Lavallée S, Perron G, Michot C, Armand M. Room temperature molten salts as lithium battery electrolyte. Electrochim Acta 2004;49(26):4583–8.
[26] Erten S, Icli S. Bilayer heterojunction solar cell based on naphthalene bisbenzimidazole. Inorganica Chim Acta 2008;361(3):595–600.
[27] Xuhong Q, Zhenghua Z, Kongchang C. The synthesis, application and prediction of stokes shift in fluorescent dyes derived from 1,8-naphthalic anhydride. Dyes Pigm 1989;11(1):13–20.
[28] Cacialli F, Friend R, Bouche CM, Le Barny P, Facoetti H, Sayer F, et al. Naphthalimide side-chain polymers for organic light-emitting diodes: band-offset engineering and role of polymer thickness. J Appl Phys 1998;83:2343–56.
[29] Singh ThB, Erten S, Günes S, Zafer C, Turkmen G, Kuban B, et al. Soluble derivatives of perylene and naphthalene diimide for n-channel organic field-effect transistors. Org Electron 2006;7(6):480–9.
[30] Saito I. Photochemistry of highly organized biomolecules: sequence-selective photoreaction of DNA. Pure Appl Chem 1992;64(9):1305–10.
[31] Tian H, He Y, Chang CP. Synthesis and spectral properties of novel laser copolymers based on modified rhodamine 6G and 1,8-naphthalimide. J Mater Chem 2000;10:2049–55.
[32] Martynski T, Mykowska K, Bauman D. Spectral properties of fluorescent dyes in nematic liquid crystals. J Mol Struct 1994;325:161–7.
[33] Lin IJB, Vasam CS. Metal-containing ionic liquids and ionic liquid crystals based on imidazolium moiety. J Organomet Chem 2005;690(15):3498–512.
[34] Gan J-A, Song QL, Hou XY, Chen K, Tian H. 1,8-Naphthalimides for non-doping OLEDs: the tunable emission color from blue, green to red. J Photochem Photobiol A: Chem 2004;162(2–3):399–406.
[35] Kolosov D, Adamovich V, Djurovich P, Thompson ME, Adachi C. 1,8-Naphthalimides in phosphorescent organic LEDs: the interplay between dopant, exciplex, and host emission. J Am Chem Soc 2002;124(33):9945–54.
[36] Sureshkumar M, Lee C-K. Biocatalytic reactions in hydrophobic ionic liquids. J Mol Catal B: Enzymatic 2009;60(1–2):1–12.
[37] Jain N, Kumar A, Chauhan S, Chauhan SMS. Chemical and biochemical transformations in ionic liquids. Tetrahedron 2005;61(5):1015–60.
[38] Wang Y, Sun Y, Song B, Xi J. Ionic liquid electrolytes based on 1-vinyl-3-alkylimidazolium iodides for dye-sensitized solar cells. Solar Energy Mater Solar Cells 2008;92(6):660–6.
[39] Barros TC, Brochsztain S, Toscano VG, Filho PB, Politi MJ. Photophysical characterization of a 1,4,5,8-naphthalenediimide derivative. J Photochem Photobiol A: Chem 1997;111(1–3):97–104.
[40] Crosby GA, Demas JN. Measurement of photoluminescence quantum yields. Review. J Phys Chem 1971;75(8):991–1024.
[41] Dawson WR, Windsor MW. Fluorescence yields of aromatic compounds. J Phys Chem 1968;72(9):3251–60.
[42] Magalhães JL, Pereira RV, Triboni ER, Filho PB, Gehlen MH, Nart FC. Solvent effect on the photophysical properties of 4-phenoxy-N-methyl-1,8-naphthalimide. J Photochem Photobiol A: Chem 2006;183(1–2):165–70.
[43] Lower SK, El-Sayed MA. The triplet state and molecular electronic processes in organic molecules. Chem Rev 1966;66(2):199–241.
[44] Lakowicz JR. Principles of fluorescence spectroscopy, part 8. New York: Kluwer Academic/Plenum Publisher; 1999.
[45] Kavarnos GJ, Turro NJ. Photosensitization by reversible electron transfer; theories, experimental evidence, and examples. Chem Rev 1986;86(2):401–49.
[46] Jones II G, Griffin SF, Choi CY, Bergmark WR. Electron donor-acceptor quenching and photoinduced electron transfer for coumarin dyes. J Org Chem 1984;49(15):2705–8.
[47] Kuang D, Klein C, Snaith HJ, H-Baker R, Zakeeruddin SM, Grätzel M. A new ion-coordinating ruthenium sensitizer for mesoscopic dye-sensitized solar cells. Inorganica Chim Acta 2008;361(3):699–706.
[48] Sahin C, Tozlu C, Ocakoglu K, Zafer C, Varlikli C, Icli S. Synthesis of an amphiphilic ruthenium complex with swallow-tail bipyridyl ligand and its application in nc-DSC. Inorganica Chim Acta 2008;361(3):671–6.
[49] Sahin C, Ulusoy M, Zafer C, Ozsoy C, Varlikli C, Dittrich T, et al. The synthesis and characterization of 2-(2′-pyridyl)benzimidazole heteroleptic ruthenium complex: efficient sensitizer for molecular photovoltaics. Dyes Pigm 2010;84(1):88–94.
[50] Ocakoglu K, Zafer C, Cetinkaya B, Icli S. Synthesis, characterization, electrochemical and spectroscopic studies of two new heteroleptic Ru(II) polypyridyl complexes. Dyes Pigm 2007;75(2):385–94.
[51] Wang P, Chai C, Chuai Y, Wang F, Chen X, Fan X, et al. Blue light-emitting diodes from mesogen-jacketed polymers containing oxadiazole units. Polymer 2007;48(20):5889–95.
[52] Bonhote P, Dias A-P, Papageogiou N, Kalyanasundaram K, Gratzel M. Hydrophobic, highly conductive ambient-temperature molten salts. Inorg Chem 1996;35(5):1168–78.
[53] Min GH, Yim T, Lee HY, Huh DH, Lee E, Mun J, et al. Synthesis and properties of ionic liquids: imidazolium tetrafluoroborates with unsaturated side chains. Bull Korean Chem Soc 2006;27(6):847–52.
[54] Yeon S-H, Kim K-S, Choi S, Lee H, Kim HS, Kim H. Physical and electrochemical properties of 1-(2-hydroxyethyl)-3 methyl imidazolium and N-(2-hydroxyethyl)-N-methyl morpholinium ionic liquids. Electrochim Acta 2005;50(27):5399–407.
[55] Kolthoff IM, Coetzee JF. Polarography in acetonitrile. II. Metal ions which have significantly different polarographic properties in acetonitrile and in water. Anodic waves. Voltammetry at rotated platinum electrode. J Am Chem Soc 1957;79(8):1852–8.
[56] Ngo HL, LeCompte K, Hargens L, McEwen AB. Thermal properties of imidazolium ionic liquids. Thermochim Acta 2000;357-358:97–102.
[57] Kosmulski M, Gustafsson J, Rosenholm JB. Thermal stability of low temperature ionic liquids revisited. Thermochim Acta 2004;412(1–2):47–53.
[58] Fredlake CP, Crosthwaite JM, Hert DG, Aki SN, Brennecke JF. Thermophysical properties of imidazolium-based ionic liquids. J Chem Eng Data 2004;49(4):954–64.
[59] Huddleston JG, Visser AE, Reichert WM, Willauer HD, Broker GA, Rogers RD. Characterization and comparison of hydrophilic and hydrophobic room

temperature ionic liquids incorporating the imidazolium cation. Green Chem 2001;3:156–64.
[60] Fox DM, Awad WH, Gilman JW, Maupin PH, De Long HC, Trulove PC. Flammability, thermal stability, and phase change characteristics of several trialkylimidazolium salts. Green Chem 2003;5:724–7.
[61] Kroon MC, Buijs W, Peters CJ, Witkamp G-J. Quantum chemical aided predictions of the thermal decomposition mechanisms and temperatures of ionic liquids. Thermochim Acta 2007;465(1–2):40–7.
[62] Singh I, Mathur PC, Bhatnagar PK, Kaur I, Bharadwaj LM, Pandey R. Study of photoluminescence quenching and DC conductivity measurements in polymer-SWNT composite films for various SWNT concentrations. Int J Nanotech 2009;6(7–8):745–52.
[63] Johansson P, Fast LE, Matic A, Appetecchi GB, Passerini S. The conductivity of pyrrolidinium and sulfonylimide-based ionic liquids: a combined experimental and computational study. J Power Sources 2010;195(7):2074–6.